Colloids and Surfaces B: Biointerfaces 220 (2022) 112963

Contents lists available at ScienceDirect

Colloids and Surfaces B: Biointerfaces

journal homepage: www.elsevier.com/locate/colsurfb

Evaluation of electrospun PCL diol-based elastomer fibers as a beneficial matrix for vascular tissue engineering

Tonghe Zhu [a,c,1], Jingjing Zhu [a,1], Shuyang Lu [b], Xiumei Mo [a,*]

[a] State Key Laboratory for Modification of Chemical Fibers and Polymer Materials, College of Biological Science and Medical Engineering, Donghua University, 2999 North Renmin Rd., Shanghai 201620, PR China

[b] Department of Cardiovascular Surgery, Zhongshan Hospital, Fudan University, The Shanghai Institute of Cardiovascular Diseases, 1609 Xietu Rd., Shanghai 200032, PR China

[c] School of Chemistry and Chemical Engineering, Shanghai Engineering Research Center of Pharmaceutical Intelligent Equipment, Shanghai Frontiers Science Research Center for Druggability of Cardiovascular Non-coding RNA, Institute for Frontier Medical Technology, Shanghai University of Engineering Science, 333 Longteng Rd., Shanghai 201620, PR China

ARTICLE INFO

Keywords:
Segmented elastomer
Electrospun fibers
Beneficial matrix
Biocompatibility
Vascular tissue engineering

ABSTRACT

The main reason for the failure of artificial blood vessel transplantation is the lack of mechanically matched materials with excellent blood compatibility. The electrospun biodegradable polyurethane (BPU) fibers with micro to nanoscale topography and high porosity similar to the natural extracellular matrix (ECM) is one of the most suitable options for vascular graft. In our recent study, we prepared a series of PCL-based BPU fibers by combining two-step solution polymerization and electrospinning. SEM, ^{1}H NMR, ATR-FTIR, XRD, TG, water contact angle, and mechanical tests were used to analyze the chemical structure, microstructure, thermal properties, surface wettability, degradation, cytocompatibility, and hemocompatibility in vitro of electrospun fibers. The results show that the synthesized H-PEUU, L-PEUU, H-PEEUU, and L-PEEUU have different crystalline properties, thus exhibiting distinctive thermal, mechanical, and degradation properties. Although the existence of the molecular structure of LDI and PEG600 in fibers can promote cell proliferation and migration unilaterally, the microstructure of the material is also the main factor affecting the biocompatibility of cells. The results suggest that the designed PCL-based degradable polyurethane electrospun fiber is expected to be applied to vascular tissue engineering.

1. Introduction

There are statistics that by 2022 there will be 300 million patients with cardiovascular and cerebrovascular diseases disease in China, of which about 42 thousand need small-diameter artificial blood vessels for bypass therapy each year [1]. Nowadays, for applicable small-diameter artificial vessels in clinically, autologous vein or artery are the gold standard. However, the lack of sufficient donors for such autologous blood vessels has limited its applications [2]. So, the most promising solution is to develop artificial blood vessels with excellent biocompatibility and safety using biomaterials. As artificial blood vessels for tissue repair, it should have not only excellent biocompatibility but also have suitable mechanical matching [3–5]. According to the characteristics of vascular tissue, a "matching" engineered vascular scaffold should be designed according to the properties of the raw material itself. The above-mentioned "matching" should include the following meanings. First, the raw materials for preparing tissue engineering vascular scaffolds should have excellent biocompatibility and definite degradation cycle. Moreover, according to the different features of autologous tissue, a three-dimensional scaffold that is biomimetic in both macroscopic and microscopic structures should be designed and prepared. Last but not least, how to make the mechanical properties of the scaffold match with the autologous vascular tissue as much as possible still remains a challenge [6–8].

Due to the limited raw materials and insufficient processing technology for preparing tissue engineering scaffolds, it is a great challenge for achieving a perfect scaffold [9–11]. Biodegradable polyurethane elastomers, which possess a diversiform chemical structure, adjustable mechanical properties [12–15], and excellent biocompatibility, are widely studied and applied in the fields of tissue engineering and drug

* Corresponding author.
E-mail address: xmm@dhu.edu.cn (X. Mo).
[1] These authors contributed equally to this work.

https://doi.org/10.1016/j.colsurfb.2022.112963
Received 2 August 2022; Received in revised form 19 October 2022; Accepted 20 October 2022
Available online 21 October 2022

release [16,17]. The soft segment in degradable polyurethane is mainly oligomers or copolymers with hydroxyl groups at both ends (such as polylactic acid (PLA) [18,19], polyglycolic acid (PGA), polycaprolactone (PCL) [20–22], polyethylene glycol (PEG) [20,22], polyethylene oxide (PEO) [23]), and the chain extender of the hard segment using degradable diol or diamine [24–26]. All in all, we can design and synthesize the molecular structure of degradable polyurethane elastomers individually according to different application requirements.

PCL is a linear polyester with excellent mechanical properties and a degradation cycle of up to two years in vivo [27]. Although, it is possible to reduce the degradation cycle of PCL by regulating the molecular weight of the polymer. However, this is not a wise choice because it will sacrifice the mechanical properties of the material[28]. In addition, unlike PLA, the degradation products of PCL rarely cause the local tissue pH imbalance, which is the main culprit in causing sterile infection [29]. Through our comparative analysis of domestic and foreign research, it is found that although PEUU has prominent mechanical properties as well as good biocompatibility for tissue engineering, it is still a class of hydrophobic materials, which greatly limits their biomedical applications [30]. Polyethylene glycol (PEG), which can be dissolved in both water and organic solvents, presents good amphiphilicity, with wide molecular weight distribution, and no immunogenicity, is a kind of end group that can be further reversed [31].

Based on the excellent performance of degradable polyurethane elastomers in tissue engineering described above, four kinds of degradable polyurethane elastomers with different structures will be synthesized and named as H-PEUU, L-PEUU, H-PEEUU, and L-PEEUU respectively using diisocyanate (HDI or LDI), PCL diol, PEG600 and putrescine as reactive monomers by a two-step solution polymerization method. Following, the fibers mats or fibers tubes will be prepared by electrospinning using the synthesized polymer elastomers with four different structures (as shown in Graphical Abstract). The chemical structure, microscopic morphology and microstructure, thermal properties, surface wettability, and degradation in vitro of the nanofibers were tested and analyzed. Further, studies on endothelial cell proliferation, migration, and other related cell biology were also carried out. Ultimately, we expect that the research results of the polymer nanofibers will be a theoretical basis for later applications for tissue regeneration.

2. Materials and methods

2.1. Synthesis of polymeric elastomer

Polymeric elastomer (synthesized with PCL diol, HDI (or LDI) as soft segments and 1, 4-butanediamine as chain extender, they are named H-PEUU, L-PEUU, H-PEEUU, and L-PEEUU, respectively) were synthesized via a two-step solution polymerization: Poly(Ɛ-caprolactone) diol (Mn=2000 g/mol) and hexamethylene diisocyanate (HDI) (or LDI) were mixed and reacted at 80 °C for 2.5 h and added with 1, 4-butanediamine (DAB) for chain extension at 40 °C for 18 h. For the synthesis of H-PEUU or L-PEUU: The molar ratio of poly(Ɛ-caprolactone) diol, hexamethylene diisocyanate (or L-lysine ethyl ester diisocyanate), and 1,4-butanediamine is 1: 2: 1. Similarly, for the synthesis of H-PEEUU or L-PEEUU: The molar ratio of poly(Ɛ-caprolactone) diol, polyethylene glycol, hexamethylene diisocyanate (or L-lysine ethyl ester diisocyanate, LDI), and 1,4-butanediamine is 0.5: 0.5: 2: 1. After the chain extension, the synthesized product was washed and purified with deionized water for three days, and freeze-dried to obtain a dry and pure polymeric elastomer. The yield of the synthesized polymeric elastomers in this experiment were all over 90%. The estimated ultimate weight average molecular weight of synthetic H-PEUU, L-PEUU, H-PEEUU, and L-PEEUU are 4.5×10^4 g/mol, 4.1×10^4 g/mol, 4.0×10^4 g/mol, 3.8×10^4 g/mol, respectively. The detailed monomer and chain extender settings are shown in Table S1.

2.2. Preparation of electrospun nanofibers

Synthetic polymeric elastomer (H-PEUU, L-PEUU, H-PEEUU, and L-PEEUU) were dissolved in 10 mL of HFIP to form a mixture with optimum concentration with vigorous stirring at room temperature for 72 h until clarified. Then, the 10 mL of the above prepared mixture solution were electrospinning to generate nanofibers according to the parameters in Table S2. The as-electrospun nanofibers were collected onto a stainless steel bar (2 mm diameter, 100 mm length, rotated at 200 rpm) or a flat aluminum foil board located 14 cm from the capillary to form nanofibers tubes or nanofibers mats, namely H-PEUU, L-PEUU, H-PEEUU, and L-PEEUU, respectively. Then nanofibers tubes and nanofibers mats were vacuumed in a desiccator for 48 h to remove residual HFIP.

2.3. Characterization and testing of synthetic polymeric elastomers, nanofibers, and nanofibers tubes

Attenuated total reflectance-Fourier transform infrared spectrometer (ATR-FITR, Thermo Nicolet, USA) was employed to characterized the chemical structure of synthetic polymeric elastomers in the range of 400–4000 cm^{-1} under a resolution of 4 cm^{-1}. The D/max-2550 PC X-ray diffractometer (Rigaku Co, Tokyo, Japan) was adopted to characterize the crystalline of nanofibers in the scanning region of 2θ= 5–60°. The differential scanning calorimetry (DSC, Q25, TA) and the thermogravimetric analysis (TGA, TGA550, TA) were performed to determine the thermal properties of the synthetic polymeric elastomer. Samples were heated from − 72–112 ℃ at 10 ℃/min in a nitrogen environment during the DSC measurements. The TGA was tested at ambient temperature and heated to 900 °C at 10 °C/min. Synthetic polymeric elastomers were characterized by ^{1}H spectrum nuclear magnetic resonance (^{1}H NMR, AVANCE-400 MHz, Bruker, Switzerland) with DMSO-d_6 as solvent.

The morphology and surface structure of electrospun nanofibers were carried out using a scanning electron microscope (SEM, Phenom XL, Netherlands) operating with sputter gold plating for 35 s at 5 mA at an accelerating voltage of 10 kV. The diameters of the electrospun nanofibers mats were measured using Image J software ((National Institutes of Health, USA)) on the basis of the SEM images. One hundred fibers diameters on different parts of the SEM images were chosen randomly, thus measuring the distribution of fibers diameters. The porosity of the mats was tested via the ethanol infiltration method. A slice of the mat was immersed in the ethanol; the volume of ethanol in the measuring cylinder before and after the nanofibers mat immersion was set as V_1 and V_2, respectively. After 15 min, the mat was removed from the ethanol, and the remaining volume was marked as V_3; the porosity of the tested membranes was calculated according to Eq. (1):

$$\text{Porosity}\left(\%\right) = \frac{V1 - V3}{V2 - V3} \times 100\% \quad (1)$$

A contact angle measuring device (JC 2000D 2 A, Shanghai Zhongchen Digital Technology Equipment Co., Ltd, China) was used to test the wettability of nanofibers mats. In this testing, 0.03 mL deionized water was added to the sample, and three different positions of the sample were taken to test the water contact angle and calculate the average value. Image-J (National Institutes of Health, USA) was adopted to determine the diameter of nanofibers.

High-precision tensile testing machine (HY-025CS, Shanghai Hengyu Instrument Co., Ltd, China) with a transducer with a load range of 0–200 N was employed to test the mechanical properties of nanofibers mats in dry conditions at room temperature strictly according to ISO 7198: 1998. Each sample was cut into a rectangle with length ×width × thickness = 50.0 mm × 10.0 mm × 0.4 mm. Finally, tensile tests were investigated at room temperature with a stretching speed of 10 mm/min. The specimens were extended until breaking under tensile force and the tensile stress-strain curves were recorded. Each test was

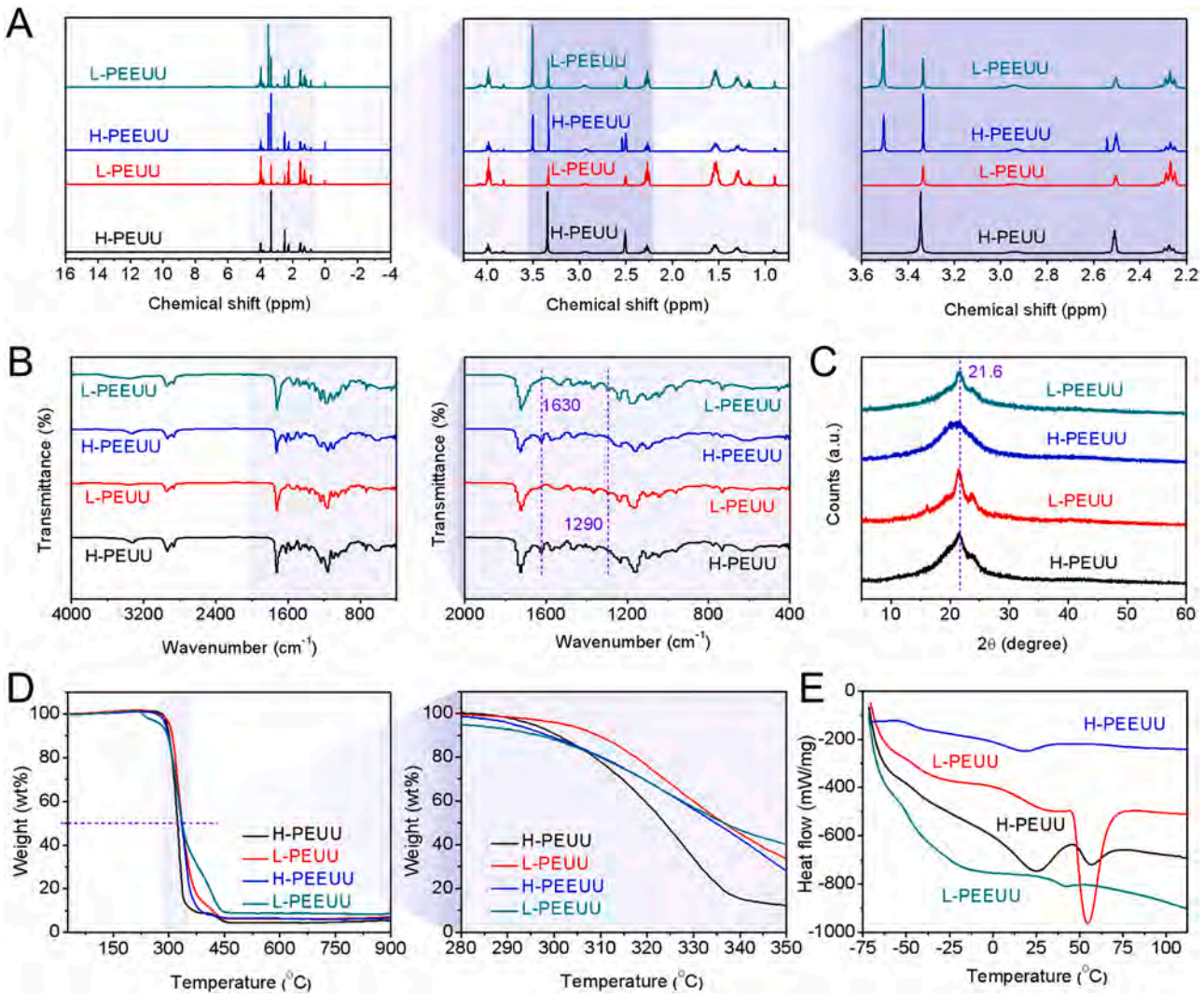

Fig. 1. (A) ^{1}H NMR spectra, (B) ATR-FTIR spectra, (C) wide-angle X-ray diffraction pattern, (D) TG curves, and (E) DSC curves of H-PEUU, L-PEUU, H-PEEUU, and L-PEEUU polymers elastomer, respectively.

repeated five times during mechanical analysis. The tensile strength, elongation at tensile strength, the representative modulus, and first order equation fitting of stress and strain within the magnification of calculating range were calculated according to the results of stress-strain.

The tensile properties circumferential direction and suture retention strengths of fibers tubes were also tested by a tensile testing machine (HY-940FS, Shanghai Hengyu Instrument Co., Ltd, China) with a sensor with a load range of 0–200 N. Radial tensile properties of fibers tubes were determined in the circumferential direction via two "L"-shaped clamps as demonstrated in Fig. S1A. Burst pressure was measured by a customized device in accordance with section 8.3.3.3 of ISO 7198: 1998.

2.4. Degradation in vitro

The degradation of the prepared nanofibers mats was measured during 24 weeks according to the well-known weight method used in PBS buffer solution in vitro. Nanofiber strips with square shape (length ×width × thickness = 10.0 mm × 10.0 mm × 0.2 mm) were placed in a 10 mL PBS (pH = 7.4) solution (PBS was changed every other week). The initial mass of the nanofibers strip was weighed before soaked in PBS. After that, the nanofiber strip was dried and weighed after taken out at the setting time point to analyze the degradation degree. The weight remaining rate was determined by Eq. (2):

$$\text{Weight remaining rate}(\%) = W_2/W_1 \times 100\% \quad (2)$$

where W_1 expresses the initial mass of the nanofibers strip; W_2 stands for the mass of the setting time point of the nanofibers strip after degradation.

The number-average molecular weight (Mn) of nanofibers before and after degradation was measured by Gel Permeation Chromatography (PL-GPC50, Agilent Technologies (China) Co., Ltd). The concentration of the sample solution for the testing was 5 mg/mL. Hexafluoroisopropanol (HFIP) was used as the mobile phase and the flow rate was set to 1 mL/min. See more experimental details in the Supporting Information.

3. Results and discussion

High-quality materials that can be used to prepare tissue engineering blood vessels should have the following characteristics: good biocompatibility is first and foremost; The structure of materials' surface is suitable for the adhesion and proliferation of host cells, as well as anticoagulation, and low immune rejection [3–5]. Moreover, it will gradually degrade or fuse with its own tissue for a certain period of time [32,33]. The degradation rate is comparable to the regeneration rate of the autologous extracellular matrix, and the degradation products are

non-toxic. It has suitable pore size and matched mechanical properties with natural blood vessels [34–36].

Up to now, there is no material that can meet the requirements of manufacturing artificial blood vessels with small diameter (less than 6 mm) in clinical practice [37–44]. This is mainly because the existing synthetic materials cannot escape the attack of the body's immune system, and the surface of the material is easy to induce coagulation and inflammatory reactions [45–48]. Biodegradable polyurethane nanofibers have excellent physical and mechanical properties and are suitable as small blood vessel materials [21,49,50]. However, the biocompatibility of polyurethane materials is far from meeting the requirements of long-term clinical implantation of small blood vessels, and it needs to be synthesized and modified [48,51,52].

Therefore, we have designed and synthesized a series of biodegradable polyurethane (H-PEUU, L-PEUU, H-PEEUU, and L-PEEUU), following electrospun into nanofibers, which with a structure of the bionic extracellular matrix exhibited matched mechanical properties (Graphical Abstract).

3.1. Characterization of synthetic polymeric elastomer

Synthetic block polyurethane materials, which with prominent mechanical properties, abundant source, as well as easily molding, have a wide range of applications in tissue engineering due to their tunable physical, chemical, biomechanical, and degradation properties. We are devoted to the study of biodegradable block polyurethane for vascular tissue. Detailedly, Biodegradable PCL and bioactive molecules were introduced into the molecular backbone of polyurethane by designing different structures of soft and hard segments and adjusting the molar ratio of synthetic monomers to synthesize biodegradable polyurethane with bioactivity and tissue inducibility. The ultimate goal is to optimize the preparation of vascular tissue engineering materials with stable comprehensive mechanical properties, processable strength, moderate surface infiltration, and excellent biocompatibility.

In this study, four synthetic polymeric elastomers were synthesized by a two-step method using PCL diol and PEG_{600} as the soft segment and HDI (or LDI) as the hard segment (Graphical Abstract A and Graphical Abstract B). The chemical structure of synthetic polymeric elastomers (H-PEUU, L-PEUU, H-PEEUU, and L-PEEUU) were investigated by ^1H spectrum nuclear magnetic resonance (^1H NMR) and attenuated total reflection Fourier transform infrared spectroscopy (ATR-FTIR), respectively (Fig. 1A and B). ^1H NMR was used to confirm the chemical structure of the synthetic polymeric elastomers. As the ^1H NMR spectra of H-PEUU, L-PEUU, H-PEEUU, and L-PEEUU shown in Fig. 1A, all the synthesized polymeric elastomers exhibited characteristic peaks at 2.50 ppm and 3.35 ppm belonging to DMSO and H_2O structures, respectively. Characteristic peak of methylene at 2.92 ppm may linked to -NCO in HDI or LDI. The strong absorption peak at 1.38 ppm may due to the methyl proton peak of ethyl ester group in LDI, while it does not appear in H-PEEUU due to the fact that the absence of this group in H-PEUU. All the above chemical shift peaks verify that PEG600, LDI, or HDI have been successfully introduced into the molecular chain of BPU.

As ATR-FTIR spectra shown in Fig. 1B, all of the four synthetic polymeric elastomers have an absorption peak at 3335 cm^{-1}, which may be the N-H characteristic absorption peak in the carbamate group (-NHCOO-). The absorption peak at 3335 cm^{-1} of L-PEUU and L-PEEUU is significantly higher than that of H-PEUU and H-PEEUU. This is mainly due to the fact that the reactivity of -NCO in HDI with -OH in PCL diol or PEG_{600} is stronger than LDI, which will lead to more -NHCOO- group formed. The absorption peak at 1100 cm^{-1} is the stretching vibration of the ether bond. The characteristic carbonyl of PCL appeared at 1730 cm^{-1}. The asymmetric and symmetric stretching vibrations of the methylene group were identified at 2860 cm^{-1} and 2950 cm^{-1}, respectively. 1720 cm^{-1} is the absorption peak of C═O on the ester group, which is consistent with the infrared spectrum of a typical polyester polyurethane. The absorption peak at 1170 cm^{-1} is the stretching vibration peak of C-O-C in the soft segment, and 1240 cm^{-1} belongs to the stretching vibration peak of -CO-O-C-. On the other hand, only H-PEUU and H-PEEUU have absorption peaks at 1630 cm^{-1}, which indicates that the presence of the side chain group $-COOC_2H_5$ in LDI makes it easier to react the -NCO group with $-NH_2$ in 1,4-butanediamine to form a broader band characteristic $\delta_{N\text{-}H}+ \upsilon_{C\text{-}N}$. Neither PCL diols and characteristic hydroxyl groups (-OH) at 3500 cm^{-1} in PEG_{600} nor a specific absorption peak of isocyanate (-NCO) at 2260 cm^{-1} in HDI (LDI) exists in the infrared spectra of the four polymer elastomers, which demonstrates that the hydroxyl groups at both ends of the PCL diol and the isocyanate groups at both ends of the HDI (LDI) have completely reacted.

The crystal structure, surface wettability, and degradation performance of polymer materials are closely related. As the main segment of BPU, PCL has strong crystallinity, slow biodegradation, and hydrophobic surface and interface, which limits the comprehensive biological properties of PCL, although it has excellent biocompatibility and outstanding mechanical properties. Therefore, much attention has been drawn to diblock copolymers using PE_{G600} and PCL diol as synthetic monomers. The wide-angle X-ray diffraction (WAXRD) pattern further confirmed the difference in crystallinity of the four synthetic polymeric elastomers (BPU) (Fig. 1C). Both the synthesized BPU and PCL have crystalline regions, two diffraction peaks, as well as the same positions of the diffraction peaks (at 2θ=21.6° and 23.6°). Compared with the diffraction peaks of PCL and PEG_{600}, the intensities of the diffraction peaks of the four synthetic polymer elastomers here are significantly weaker, mainly due to both PCL and PEG_{600} being crystalline polymers and the molecular chain being relatively compliant and more prone to movement. More specifically, the peaks of H-PEUU and L-PEUU were sharper than H-PEEUU and L-PEEUU, respectively. This result confirmed that the addition of PEG_{600} altered the crystallinity of the synthesized BPU, which is mainly due to the fact that PCL is a polymer with a more flexible molecular chain, and the movement of the molecular chain is easier than that of PEG_{600}, which is reflected in the XRD spectrum as sharp diffraction peaks.

Since the predesigned nanofibers tubular grafts were prepared by electrospinning, it is very indispensable to test the TG and DTG of the synthesized polymeric elastomers. The TG and DTG curves present the thermal stability of polymeric elastomers were shown in Fig. 1D. The TG and DTG curves also present two-stage thermal decomposition during the thermal degradation. The first is thermal decomposition of urethane and urea bonds. And the other one is due to the decomposition of soft segments. The main molecular chain of synthetic polymeric elastomers was decomposed rapidly during 210–380 ℃ hot environment. The thermal degradation temperatures of the four polymer elastomers are generally in the range of 265–275 ℃, and the 50% degradation mass temperature is near 350 ℃, indicating that the four main polymer chains have similar molecular structures. Nevertheless, as in Fig. 1D, the 50% weight loss of PEEUU increased slightly than that of PEUU, which might be explained as the introduction of PEG_{600} in the soft segment thus enhanced the thermal stability of the polyurethane elastomer, which is related to PEG_{600} is a crystalline polymer, its high crystallinity makes the molecular chain arrangement very regular, the crystalline area is not easy to change due to the external heating environment. Compared L-PEUU (L-PEEUU) with H-PEUU (H-PEEUU), L-PEUU (L-PEEUU) present the higher thermal degradation temperatures than H-PEUU (H-PEEUU). The reason for the above phenomenon may be that L-PEUU and L-PEEUU both have a side chain $-COOC_2H_5$ in the molecule, which enhances the hydrogen bond interaction in the molecular chain.

Differential scanning calorimetry (DSC) thermogram of H-PEUU, L-PEUU, H-PEEUU, and L-PEEUU was shown in Fig. 1E. The results showed that the glass transition temperature (T_g) of H-PEUU, L-PEUU, H-PEEUU, and L-PEEUU were − 52.68 ℃, − 53.15 ℃, − 52.85 ℃, and − 55.04 ℃, respectively. All the synthesized polymeric elastomers were presented with low T_g, which attributed to the PCL in soft segment (the T_g of PCL is around −60 ℃). As presented in the results of Fig. 1E, the T_g

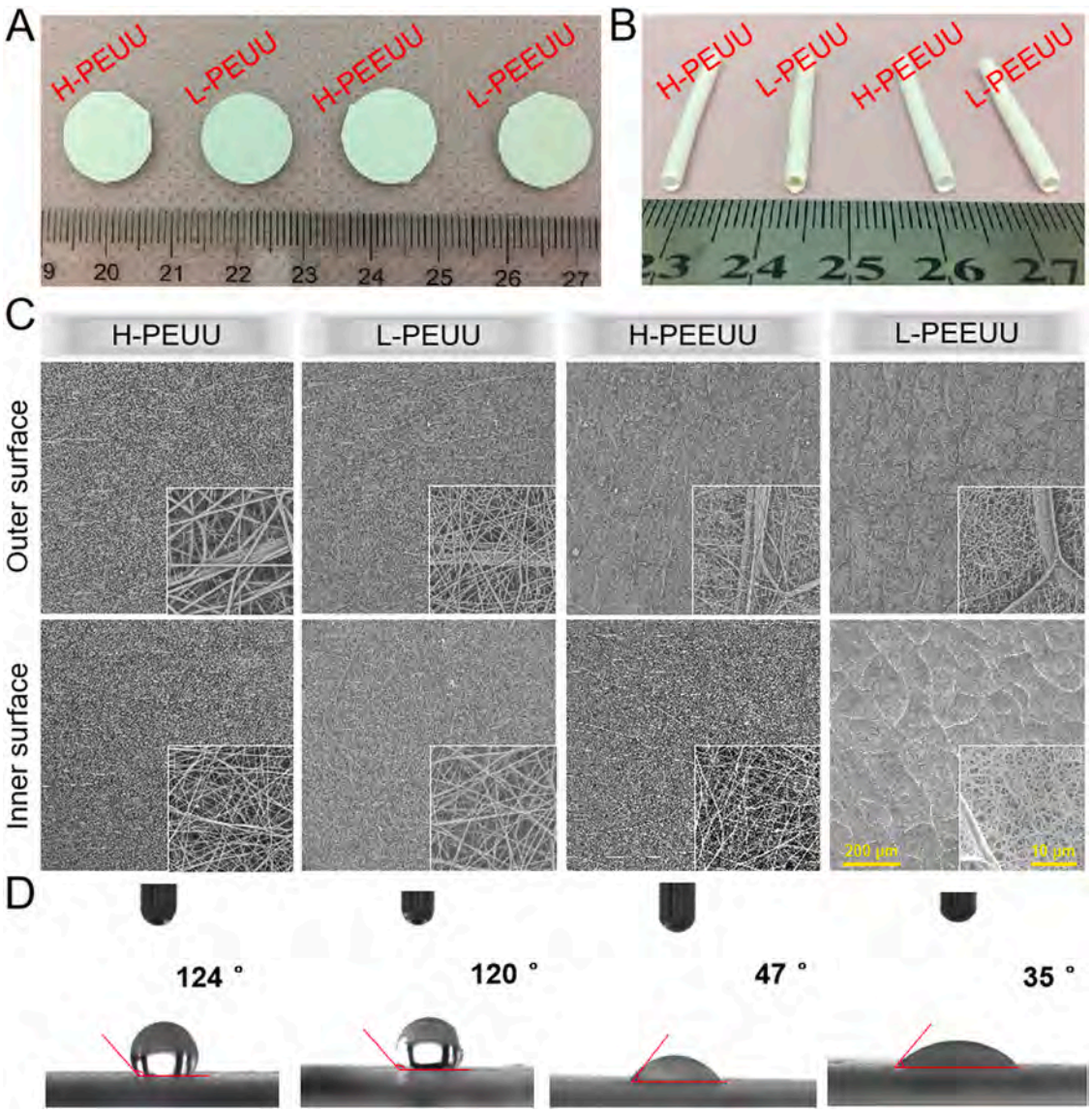

Fig. 2. (A) and (B) The digital photos of H-PEUU, L-PEUU, H-PEEUU, and L-PEEUU fibers mats and fibers tubes, respectively; (C) Outer surface and inner surface SEM images of the electrospun H-PEUU, L-PEUU, H-PEEUU, and L-PEEUU fibers, respectively; (D) Water contact angle of H-PEUU, L-PEUU, H-PEEUU, and L-PEEUU fibers mats at the 5 s time point, respectively.

of BPU with PEG chain segment was present at lower temperature than that without PEG chain segment, respectively. Moreover, when LDI is segmented into a molecular chain, the T_g of L-PEUU and L-PEEUU showed lower temperatures than H-PEUU and H-PEEUU, respectively, which may be ascribed to the asymmetry of the LDI structure that hinders the accumulation of hard segments. In addition, the melting temperatures of polymers containing PEG_{600} as a soft segment was higher than those without PEG_{600}, was due to the melting of PCL crystals. Detailedly, the presence of PEG_{600} enhanced the microphase separation of the soft segment and thus affected its crystallinity, which is also in accord with the results of WAXRD in Fig. 1C. Moreover, the PEG_{600} in the soft segment enhances the natural conformation of BPU itself, which makes the BPU molecular chain possessed less stretchable and more rigid, and reduced the thermal shock of groups within the molecule. Therefore, it was confirmed that all the four synthetic polymeric elastomers in this research presented a rubbery state at room temperature. It was also noted from the results that the structure of BPU chain had obvious influence on the crystallinity of polymers.

3.2. Microstructure and surface wettability of nanofibers

Due to the high hydrophilicity of PEG, it is easy to form a water film on its surface and inhibit protein adsorption and platelet adhesion. Therefore, PEG is often used as a modifier on the surface of biomaterials and is fixed on the surface of biomaterials via such as grafting, surface coating, and cross-linking block copolymerization to improve the blood compatibility of the material surface.

In order to improve the application of BPU in small-diameter tissue-engineered blood vessels, it is necessary to improve the hemocompatibility and histocompatibility of vascular grafts. We spun the synthesized BPU into small diameter blood artificial blood vessels with a diameter of 2 mm by electrospinning technology, and studied and analyzed the effects of different synthetic monomers on the surface morphology, microscopic morphology, and surface wettability of vascular grafts. Macroscopically, the scaffold could maintain its laminar or tubular shape after being peeled from flat aluminum foil and the steel bar, respectively (Fig. 2A and B). We obtained tubular scaffolds with a length of 20 mm and an inner diameter of 2 mm (Fig. 2B). Both the outer surface and inner surface morphology of the electrospun fibers tubes

Table 1
Mean diameter and porosity of H-PEUU, L-PEUU, H-PEEUU, and L-PEEUU fibers, respectively. (data are representatives of independent experiments and all data are given as mean ± SD, n = 5).

Samples	H-PEUU	L-PEUU	H-PEEUU	L-PEEUU
Fibers Diameter (μm)	3.26 ± 0.33	2.96 ± 0.45	1.83 ± 0.31	1.05 ± 0.28
Porosity (%)	72.1 ± 1.35	75.4 ± 2.07	78.3 ± 2.11	83.4 ± 1.98

were observed by SEM and it was found that the diameters of the four electrospun polymers were distributed between 600 and 800 nm (Fig. 2C). The diameter distribution of each group of fibers was different (Table 1). The statistical datas of diameter showed that the average diameter of H-PEUU, L-PEUU, H-PEEUU, and L-PEEUU groups were 3.26 ± 0.33, 2.96 ± 0.45, 1.83 ± 0.31, and 1.05 ± 0.28 μm. The diameter of H-PEUU group was coarse but evenly distributed. However, we also found that the average diameter decreased and porosity increased from 3.26 to 1.05 μm and 72.1–83.4% as the presence of PEG and LDI in the molecular chainr component increases (Table 1). Moreover, compared with the other three groups, the fiber distribution of H-PEUU is more uniform, smooth and no protrusions. A large number of crude fibers or clusters of aggregated fibers were found among SEM images of L-PEUU, H-PEEUU, and L-PEEUU groups. Moreover, a large number of unfiberized polymer microspheres were found on SEM images of both H-PEEUU and L-PEEUU. Even more, there is a state of adhesion between L-PEEUU fibers. This is mainly because the side chain group -$COOC_2H_5$ of LDI is a weakly negatively charged group. During the electrospinning process, the negative high voltage of more than ten thousand volts produces a small amount of electrostatic repulsion on the surface of the material, which causes some fibers to "squirt" in the electric field. On the other hand, compared with polymers without PEG600, the higher crystalline region of the polymer containing PEG600 in the soft segment limits the dispersion of polymer molecules in the solution, which destroys the spinnability of both H-PEEUU and L-PEEUU [17,18,24–26]. As shown in Fig. 2D, the water contact angle values of H-PEUU, L-PEUU, H-PEEUU, and L-PEEUU were 124°, 120°, 47°, and 35° at 5 s, respectively. It can be found that no matter how rough the fiber surface is, the contact angle of the polymer nanofibers containing PEG600 presented significantly smaller water contact angle. In brief, the above results show that the main factor affecting the surface wettability of BPU fiber mat is the chemical properties of the material itself.

3.3. Mechanical properties

As a vascular tissue engineering scaffold material, which was a biomimetic extracellular matrix, the spun nanofibers should be able to provide temporary mechanical support for the regeneration of vascular tissue and maintain the potential space for the formation of new tissue. Tensile stress-strain curves of H-PEUU, L-PEUU, H-PEEUU, and L-PEEUU, and related tensile machinery performance test results are shown in Fig. 3 and Table 1. We have found that the introduction of PEG600 and LDI in the molecular chain significantly reduced the maximum tensile strength and maximum tensile strain of BPU fibers. It is generally believed that the presence of side chains in the molecules of fiber materials makes the entanglement of molecular bonds more complicated, thereby improving the mechanical properties of fiber materials. However, some previous studies claimed that the weakly positively charged groups on the molecular side chain could form intermolecular hydrogen bonds with the electrophilic interaction between the electrons exposed on the carbonyl group of the molecular main chain, thus showing the macroscopically enhanced mechanical properties of the fiber material. The molecule side chains -$COOC_2H_5$ in both L-PEUU and L-PEEUU have a weak negative charge, which will

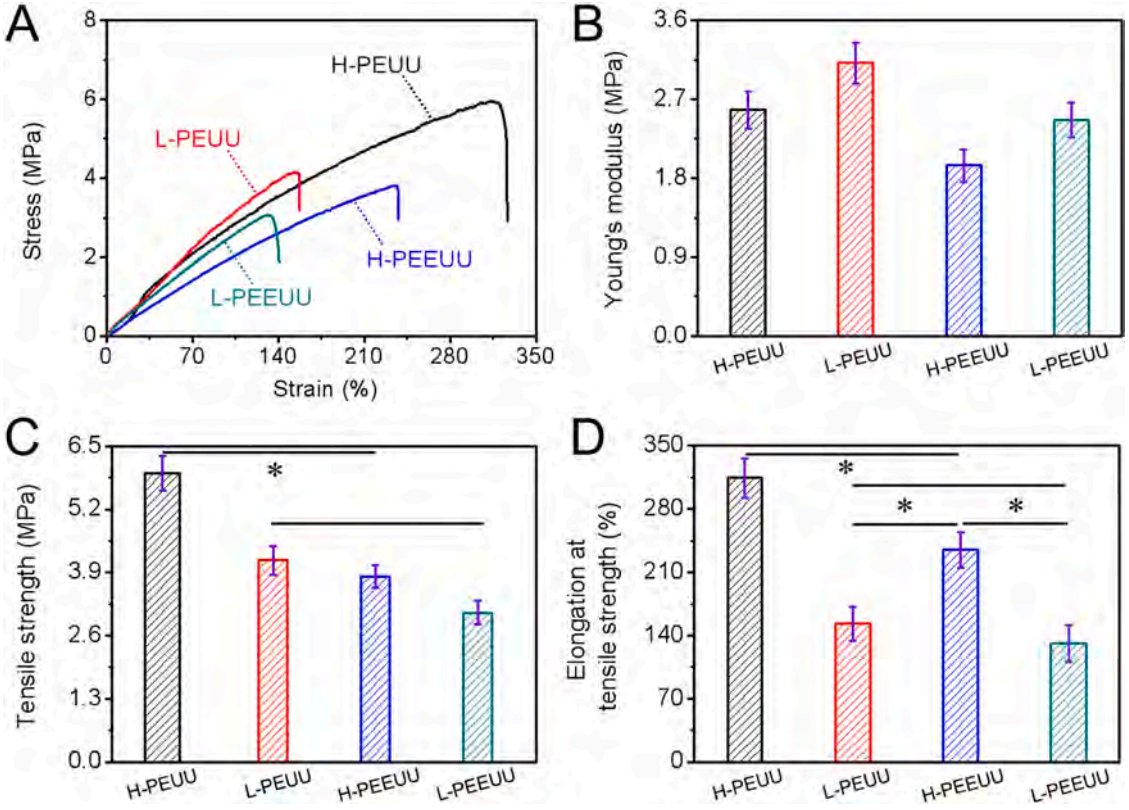

Fig. 3. Mechanical properties of prepared H-PEUU, L-PEUU, H-PEEUU, and L-PEEUU nanofibers mats, respectively: (A) Representative stress-strain curves; (F) Young's modulus; (C) Tensile strength; (D) Elongation at tensile strength. (Data are representatives of independent experiments and all data are given as mean ± SD, n = 5; * $p < 0.05$).

Table 2
Tensile properties of H-PEUU, L-PEUU, H-PEEUU, and L-PEEUU nanofibers (data are representatives of independent experiments and all data are given as mean ± SD, n = 5).

Sample	Stress (MPa)	Strain (%)	Young's modulus (MPa)
H-PEUU	5.9 ± 0.4	314.2 ± 21.3	2.6 ± 0.2
L-PEUU	4.2 ± 0.3	153.2 ± 18.7	3.1 ± 0.2
H-PEEUU	3.8 ± 0.2	234.98 ± 19.8	1.9 ± 0.2
L-PEEUU	3.1 ± 0.2	131.7 ± 20.0	2.5 ± 0.2

produce a electrostatic repulsion effect with the electrons exposed on the carbonyl group of the main chain of the molecule, that leads to a dispersed state for L-PEUU and L-PEEUU molecular chain. The above phenomena will lead to the deterioration of the mechanical properties of BPU. Combining the chemical structure and crystal structure and comparing the mechanical properties of these four polymer nanofiber membranes, we also believe that the existence of a large number of crystalline regions of PEG600 is the primary factor for the reduction of the maximum stress of the nanofiber membrane. As shown in Table 2, the maximum stresses of H-PEEUU and L-PEEUU are 3.8 MPa and 3.1 MPa, respectively, which are significantly smaller than 5.9 MPa of H-PEUU. In addition, the maximum strain data of the four nanofibers shown in Table 2 and the maximum strain variation trend shown in Fig. 3D also indicate that the intermolecular electrostatic repulsion produced by the side chain -$COOC_2H_5$ and the existence of the PEG600 crystal region are responsible for the weakening of the elasticity of BPU fibers. Finally, the low modulus of the four nanofiber mats is shown in Fig. 3B, which is also the basic feature of degradable poly(ester-urethane)urea with PCL as the main segment.

Radial tensile properties of fibers tubes are shown in Fig. S1A. Fibers tubes were squashed into rectangle shapes for axial tensile testing. Representative tensile stress-strain curves of fibers tubes in the dry state are shown in Fig. S1B. The stress-strain profile of the four fiber tubes is similar to that of the fiber mats, respectively. As the results in Fig. S1C and Fig. S1D, H-PEUU fibers tube showed comparable suture retention strength and burst pressure to the other groups. The suture retention strength and burst pressure value of grafts were much greater than those of human mammary artery (about 1.5 $\times 10^3$ mmHg) and saphenous vein (approximately 2.0 $\times 10^3$ mmHg), indicating that they are mechanically adequate for surgical procedures and robust enough to endure blood

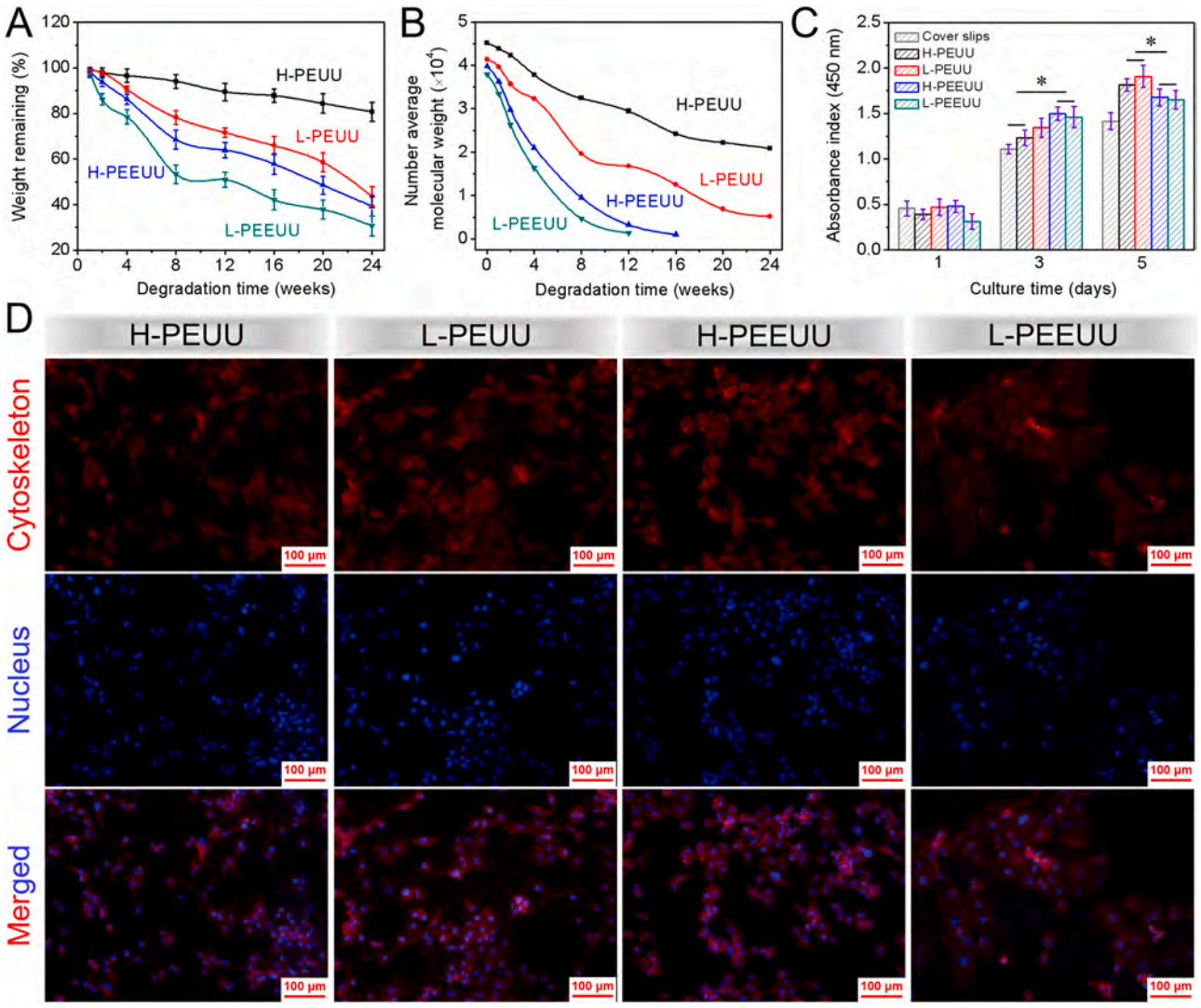

Fig. 4. (A) Mass remaining and (B) effect of biodegradation time on the number average molecular weight of H-PEUU, L-PEUU, H-PEEUU, and L-PEEUU fibers mats after degradation in PBS; (C) CCK-8 assay of the proliferation viability of HUVECs cultured onto cover slips, H-PEUU, L-PEUU, H-PEEUU, and L-PEEUU fibers mats, respectively; (D) Fluorescence microscopy images of HUVECs cultured onto H-PEUU, L-PEUU, H-PEEUU, and L-PEEUU fibers mats with labeling of cytoskeleton and nucleus after 3-day culture, respectively. (The nuclei are stained blue by DAPI and the cytoskeletons are stained red by rhodamine-conjugated phalloidin; Data are representatives of independent experiments and all data are given as mean ± SD, n = 5; * $p < 0.05$).

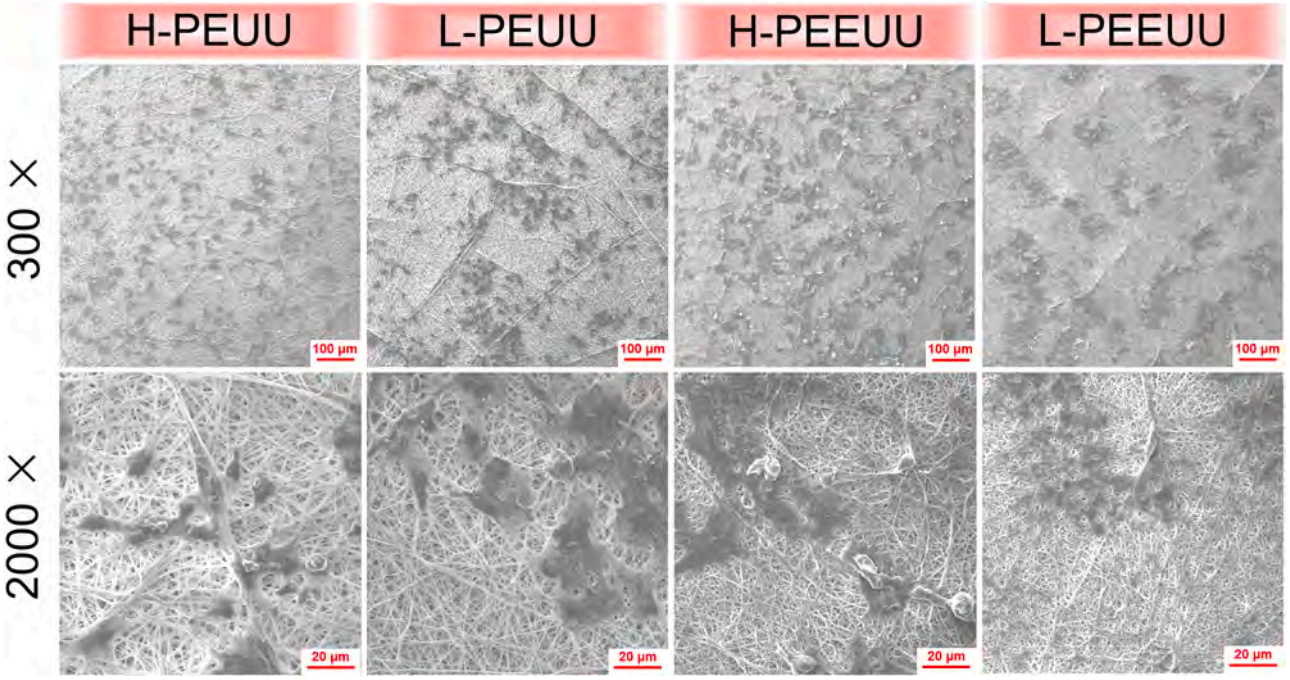

Fig. 5. SEM images of HUVECs grown onto H-PEUU, L-PEUU, H-PEEUU, and L-PEEUU fibers mats after 3-day culture and magnified 300 times and magnified 2000 times, respectively.

pressure [53].

3.4. Degradation, cytocompatibility, and hemocompatibility in vitro

The degradation percentages of spun fibers mats in PBS buffer solution are shown in Fig. 4A. Under the action of PBS hydrolysis, the H-PEUU fiber mats degraded only about 16% in 24 weeks, while the other three groups of fiber mats degraded significantly faster than the H-PEUU nanofiber mats. The degradation characteristics of the fiber mat are not only related to the chemical properties of the material itself but also to the microstructure of the fiber mat. Combined with Fig. 2C, the fibers that make up the L-PEUU fiber mat have some relatively thick fiber clusters, which will increase the pore size of the L-PEUU fiber mat, and the existence of large pore size will inevitably enhance the infiltration of the PBS solution into the fiber mat, which will accelerate the degradation of L-PEUU fiber mats. In addition, the existence of PEG600 molecular segments in BPU increases the hydrophilicity of the fiber itself, and a large number of water molecules will enter the molecular chain network, thereby accelerating the degradation of the fiber itself. This has also been reported in previous studies. For example, Guan et al. have synthetized poly(ester-urethane) urea (PEUU) and poly(ether-ester-urethane) urea (PEEUU) with PCL diol and PCL-PEG-PCL diol as soft segments, respectively. Degradation in vitro indicated that the degradation rate of PEEUU in PBS was two times faster than that of PEUU[22].

The degradation of the fiber mat must be accompanied by a decrease in the molecular weight of the material. Fig. 4B presents the changes in the number-average molecular weight of the four nanofiber materials during the degradation process. Consistent with the residual mass percentage of degradation, after 24 weeks of degradation, the number-average molecular weight of the H-PEUU fiber material decreased from 4.5×10^6 to 2.3×10^6, and the degradation rate was significantly slower than that of the other three nanofibers.

In order to test the biocompatibility of the four spun fiber materials, the proliferation experiments of HUVECs were performed on H-PEUU, L-PEUU, H-PEEUU, and L-PEEUU fiber mats, respectively. It can be found from Fig. 4C, the number of HUVECs in both the experimental group and control groups increased with the increase of culture time. The cells in each group had an obvious tendency to proliferate from the first day to the third day, indicating that the cells have been able to adapt to the surrounding microenvironment and achieve the best growth state at this time. On the fifth day, compared with the proliferation activity of the cells four days ago, the cells at this time had covered the entire fiber mat, and the proliferation was not obvious. This may be due to the contact between the cells, which presents an inhibitory effect on the continued proliferation and spreading of the cells.

Overall, in the early stage of cell proliferation, the wettability of the fiber material itself has a great impact on cell viability. For example, the ability to promote cell proliferation of hydrophilic H-PEEUU and L-PEEUU was greater than other groups on the third day. In the following stage, when the HUVECs have almost completely covered the surface of fiber mats, the effect of "contact inhibition of growth" between cells is prominent. The cells will continue to proliferate and grow into the inner fiber mat, based on the suitable pore structure of fibers mats. For example, the absorbance of H-PEUU and L-PEUU fiber mats with relatively uniform and regular fiber structure on the fifth day is greater than that of H-PEEUU and L-PEEUU. Since the cells were not full on the third day, the corresponding cytoskeleton-nucleus fluorescence staining (Fig. 4D) and cytoskeleton electron microscope (Fig. 5) showed only the apparent morphology of the cells. In conclusion, the cells on the four fiber mats had good morphology, obvious pseudopodia, and the overall spindle shape, and some cells had formed a small-scale cell community, which was in line with the normal proliferation behavior of HUVECs.

Cell adhesion, migration and proliferation are interrelated behaviors. Before the cells adhere to the fibers, they will predict the process of the material. If the cells have a rejection effect on the material, the tendency to migrate and adhere to the material will be weakened. The basis of the cell's prediction of the material is mainly according to whether the material itself has a recognition site that binds to the outside of the cell membrane. Both Figs. 6A and S2 show fluorescent staining images of HUVECs cultured onto H-PEUU, L-PEUU, H-PEEUU, and L-PEEUU fiber mats after 48 h migration, respectively. The results showed that HUVECs migrated more from both sides of the migration zone to the migration zone on the H-PEUU and H-PEEUU fiber mats than the other two groups. In addition, the shape of HUVECs in the migration zone

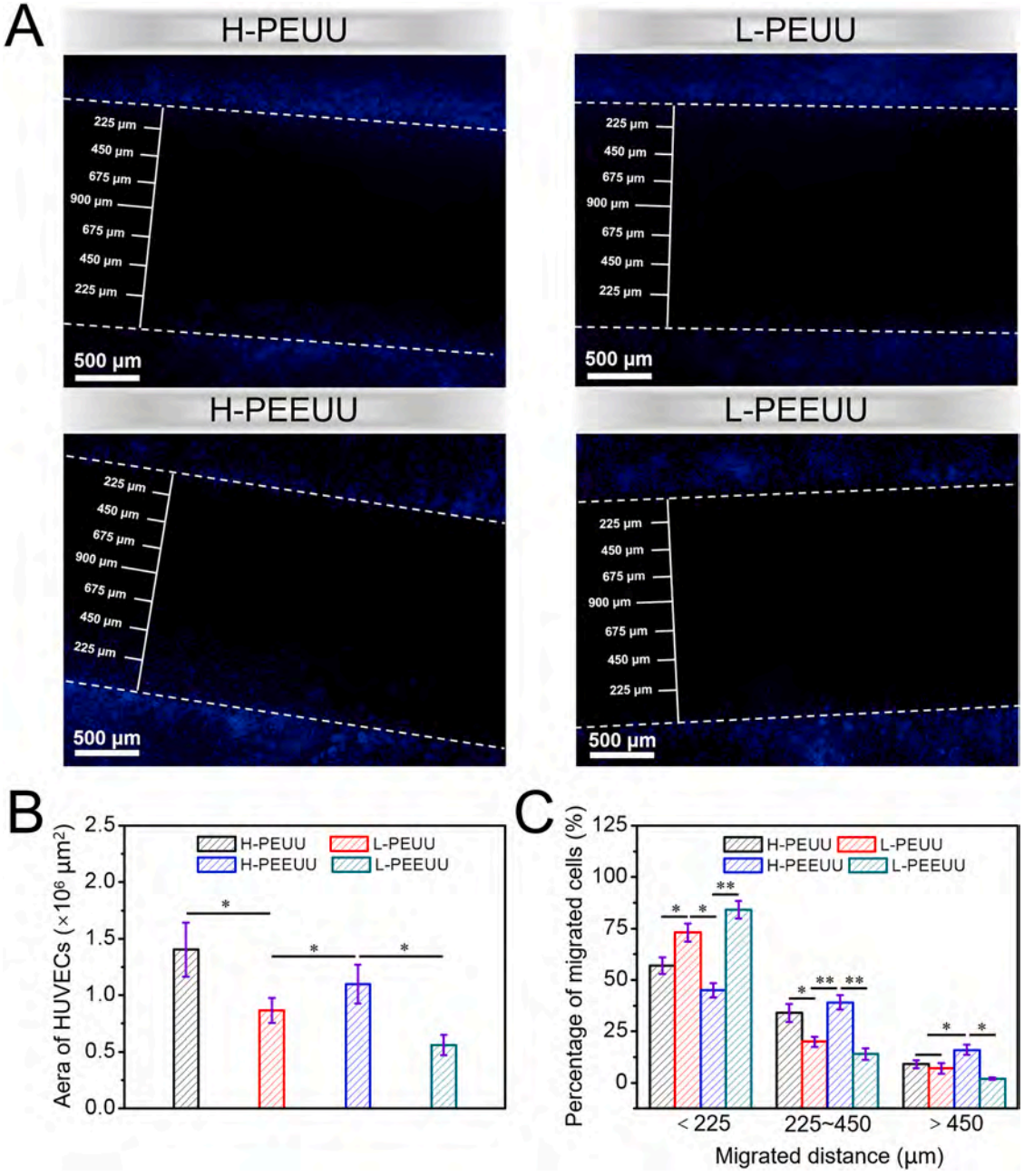

Fig. 6. Migration assay of HUVECs seeded onto H-PEUU, L-PEUU, H-PEEUU, and L-PEEUU fibers mats after incubation of the cells for 48 h, respectively: (A) With labeling of nucleus (blue) using DAPI; (B) Quantitative spreading area measurements of HUVECs on different fiber mats after culturing for 48 h; (D) Percentage of migrated HUVECs at most 225 μm, 225–450 μm, beyond 450 μm after 48 h culture. (Data are representatives of independent experiments and all data are given as mean ± SD, n = 5; ** $p < 0.01$, * $p < 0.05$).

showed obvious polypseudopodia and spindle shape, while most of the HUVECs in the non-migration zone still retained the round shape as the shape of the early stage of cell growth. We also quantified the migratory capacity of cells on the above four fiber mats. The test of cell migration ability included two aspects: quantification of the cell area in the migration zone (Fig. 6B) and the percentage of cells at different migration distances to the total migrated cells (Fig. 6C). In quantitative statistics as shown in Fig. 6C, it can be found that the H-PEEUU group has the highest proportion in the range of migration distance greater than 450 μm, which proves that the HUVECs in this group have the strongest cell migration ability, that is, the chemotactic attraction of H-PEEUU nanofibers to cells. We also believe that the smooth and regular fiber structure can maximize the retention of various nutrients, which were produced by cell metabolism in the process of cell growth and were more suitable for the later proliferation, migration and growth of host cells. As in the H-PEUU group, most of the cells were concentrated in the mid and close-range migratory zone, although HUVECs were more numerous in the migratory zone than in the other three groups. Therefore, the HUVECs grown on H-PEUU fiber mats were mainly proliferative. All in all, the process of cell growth and spreading is a coordinated process of cell adhesion, migration, and proliferation, whose ultimate goal is to achieve rapid in situ cells on the surface of the material, which will achieve the purpose of effective tissue regeneration and construction.

As a potential material for artificial blood vessels, BPU nanofibers are ceaselessly in contact with blood. Therefore, blood compatibility is also one of the important factors affecting the use of BPU. The correlation analysis results of the hemolysis experiments are shown in Fig. 7A. The value of the ordinate represents the absorbance, and the greater the

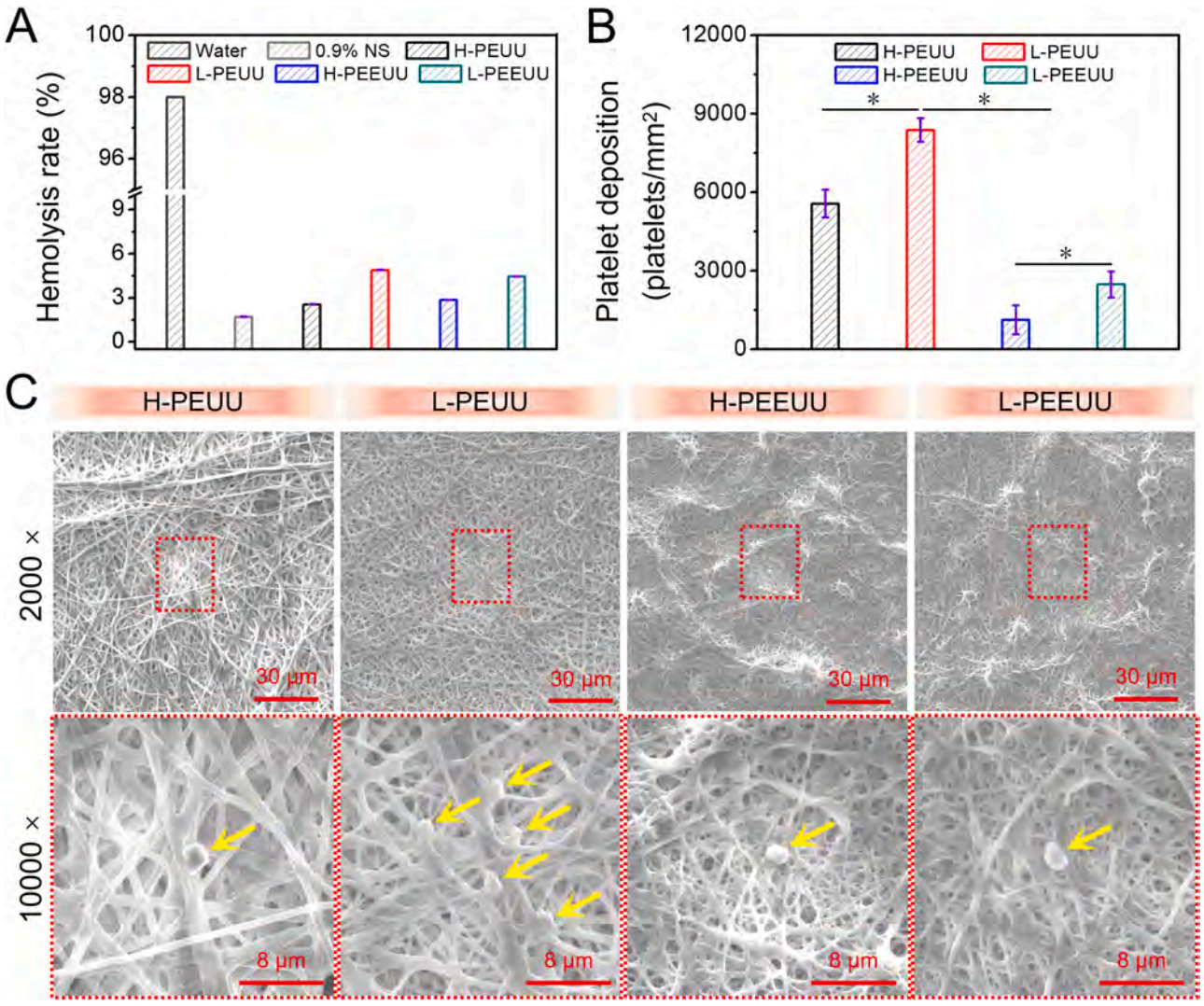

Fig. 7. (A) Quantification of relative hemolysis rate of electrospun H-PEUU, L-PEUU, H-PEEUU, and L-PEEUU fibers mats. Water (+) and 0.9% normal saline (NS) (-) were used as positive and negative control, respectively; (B) and (C) Platelet deposition determined by lactate dehydrogenase assay and SEM images. (Yellow arrows show the platelets; Data are representatives of independent experiments and all data are given as mean ± SD, n = 5; * $p < 0.05$).

absorbance means the higher the heme content in the centrifuged supernatant in the hemolysis experiment. That is, the greater the degree of damage and rupture of red blood cells during the hemolysis test, the more severe the hemolysis. The content of heme in the supernatant of the centrifuge tube in the experimental group was significantly different from that in the positive control group (distilled water) (***$p < 0.001$), while similar to the negative group (0.9% normal saline). The supernatants in the centrifuge tubes of the four experimental groups were all present transparent and clear, indicating that the H-PEUU, L-PEUU, H-PEEUU, and L-PEEUU fibers won't cause acute hemolysis after transplantation. The solution in the positive control group was blood red, indicating that the red blood cells in this group were basically destroyed, while the negative control group did not have this phenomenon. It can be seen from the hemolysis rate data in Fig. 7A that the hemolysis rates of the negative control group and the four experimental groups were all less than 5%, which further proved the hemolysis safety of the four fiber mats. The above data are also in line with the safety regulations of international standards for materials or devices that come into contact with blood.

The adhesion and activation of platelets on the surface of the material induce the coagulation response and releases substances that accelerate the coagulation response. The urethane structure of polyurethane makes it easy to generate a microphase-separated structure, which is similar to the structure of the cell wall and is less likely to cause substantial antiplatelet adhesion. Observing and calculating the adhesion quantity and morphological changes of platelets is an important index to evaluate the anticoagulant properties of materials. As shown in Fig. 7B and C, after PEG600 was used as one of the monomer blocks for synthesizing BPU, the platelet adhesion was significantly reduced, and the morphology mainly wasinactive round without pseudopodia. Quantitative analysis of lactate dehydrogenase assay (LDH) further confirmed the visual observation (Fig. 7B). In addition, we also found that only few platelets can be seen on H-PEEUU and L-PEEUU fiber mats, while the adhesive platelets on both H-PEUU and L-PEUU fiber mats are significantly higher. In particular, the amount of platelet adhesion on the L-PEUU fiber mat is the largest. The chemical properties of the fiber surface are key factors affecting platelet adhesion. The hydrophobic L-PEUU fiber molecular chain does not have a PEG segment that can form a hydration film, so it is easier to induce platelet aggregation. Moreover, due to the charged -$COOC_2H_5$ groups on the surface of L-PEUU fibers, it is more likely to cause platelet aggregation, which leads to a large number of platelet aggregation on the surface of L-PEUU fibers (Fig. 7C).

4. Conclusion

In the present study, a series of PCL-based polyurethane elastomers were synthesized by two-step solution polymerization method using PCL diol, HDI, LDI, and PEG600 as monomers, respectively. Then, the synthetic four elastomers were electrospun into fibers mats with different fibers structures. The results indicated that the presence of PEG600 in the BPU soft segment makes the BPU easier to crystallize. Due to the hydrogen bond strengthening effect in LDI type BPU, its melting point and thermal stability are stronger than HDI type BPU. Moreover, the presence of PEG600 and LDI in soft segment of BPU both reduced the spinnability of the polymer, while the stress and strain of the nanofibers were significantly reduced, but still met the requirements for vascular scaffolds. On the other hand, the presence of PEG600 promoted the degradation of the L-PEEUU nanofiber mat, which increased its degradation rate from 18% to 70% at week 24. Most importantly, we also found that the regular and uniform morphology of the fibers has a positive effect on cell proliferation and migration. Finally, in vitro platelet adhesion experiments showed that the presence of PEG600 in BPU could effectively inhibit platelet adhesion.

Declaration of Competing Interest

The authors declare that they have no known competing financial interests or personal relationships that could have appeared to influence the work reported in this paper.

Data availability

No data was used for the research described in the article.

Acknowledgments

The authors sincerely appreciate projects sponsored by the National Natural Science Foundation of China (31470941).

Appendix A. Supplementary material

Supplementary data associated with this article can be found in the online version at doi:10.1016/j.colsurfb.2022.112963.

References

[1] W. Wang, Y. Liu, J. Liu, P. Yin, L. Wang, J. Qi, J. You, L. Lin, S. Meng, F. Wang, M. Zhou, Mortality and years of life lost of cardiovascular diseases in China, 2005-2020: empirical evidence from national mortality surveillance system, Int. J. Cardiol. 340 (2021) 105–112.
[2] R.Y. Kannan, H.J. Salacinski, P.E. Butler, G. Hamilton, A.M. Seifalian, Current status of prosthetic bypass grafts: A review, J. Biomed. Mater. Res. Part B Appl. Biomater. 74B (2005) 570–581.
[3] Y. Li, Y. Xiao, C. Liu, The horizon of materiobiology: a perspective on material-guided cell behaviors and tissue engineering, Chem. Rev. 117 (2017) 4376–4421.
[4] X. Wang, M. Jiang, Z. Zhou, J. Gou, D. Hui, 3D printing of polymer matrix composites: A review and prospective, Compos. Part B Eng. 110 (2017) 442–458.
[5] G. Narayanan, V.N. Vernekar, E.L. Kuyinu, C.T. Laurencin, Poly(lactic acid)-based biomaterials for orthopaedic regenerative engineering, Adv. Drug Deliv. Rev. 107 (2016) 247–276.
[6] C. Xu, Y. Bai, S. Yang, H. Yang, D.A. Stout, P.A. Tran, L. Yang, A versatile three-dimensional foam fabrication strategy for soft and hard tissue engineering, Biomed. Mater. 13 (2018).
[7] Y. Qi, H. Wang, K. Wei, Y. Yang, R.-Y. Zheng, I.S. Kim, K.-Q. Zhang, A review of structure construction of silk fibroin biomaterials from single structures to multi-level structures, Int. J. Mol. Sci. 18 (2017).
[8] R.D. Abbott, E.P. Kimmerling, D.M. Cairns, D.L. Kaplan, Silk as a biomaterial to support long-term three-dimensional tissue cultures, ACS Appl. Mater. Interfaces 8 (2016) 21861–21868.
[9] M. Mohammadi, S.A.M. Shaegh, M. Alibolandi, M.H. Ebrahimzadeh, A. Tamayol, M.R. Jaafari, M. Ramezani, Micro and nanotechnologies for bone regeneration: Recent advances and emerging designs, J. Control. Release 274 (2018) 35–55.
[10] E.A. Makris, A.H. Gomoll, K.N. Malizos, J.C. Hu, K.A. Athanasiou, Repair and tissue engineering techniques for articular cartilage, Nat. Rev. Rheumatol. 11 (2015) 21–34.
[11] F.P.W. Melchels, M.A.N. Domingos, T.J. Klein, J. Malda, P.J. Bartolo, D. W. Hutmacher, Additive manufacturing of tissues and organs, Prog. Polym. Sci. 37 (2012) 1079–1104.
[12] H.-Y. Mi, X. Jing, B.N. Napiwocki, B.S. Hagerty, G. Chen, L.-S. Turng, Biocompatible, degradable thermoplastic polyurethane based on polycaprolactone-block-polytetrahydrofuran-block-polycaprolactone copolymers for soft tissue engineering, J. Mater. Chem. B 5 (2017) 4137–4151.
[13] F. Montini-Ballarin, P.C. Caracciolo, G. Rivero, G.A. Abraham, In vitro degradation of electrospun poly(L-lactic acid)/segmented poly(ester urethane) blends, Polym. Degrad. Stab. 126 (2016) 159–169.
[14] C. Wang, Y. Zheng, Y. Sun, J. Fan, Q. Qin, Z. Zhao, A novel biodegradable polyurethane based on poly(3-hydroxybutyrate-co-3-hydroxyvalerate) and poly (ethylene glycol) as promising biomaterials with the improvement of mechanical properties and hemocompatibility, Polym. Chem. 7 (2016) 6120–6132.
[15] H. Bergmeister, N. Seyidova, C. Schreiber, M. Strobl, C. Grasl, I. Walter, B. Messner, S. Baudis, S. Froehlich, M. Marchetti-Deschmann, M. Griesser, M. di Franco, M. Krssak, R. Liska, H. Schima, Biodegradable, thermoplastic polyurethane grafts for small diameter vascular replacements, Acta Biomater. 11 (2015) 104–113.
[16] D. Jovanovic, F.V. Roukes, A. Loeber, G.E. Engels, W. van Oeveren, X.J.G. van Seijen, M.J.A. van Luyn, M.C. Harmsen, A.J. Schouten, Polyacylurethanes as novel degradable cell carrier materials for tissue engineering, Materials 4 (2011) 1705–1727.
[17] P. Punnakitikashem, T. Danh, J.U. Menon, K.T. Nguyen, Y. Hong, Electrospun biodegradable elastic polyurethane scaffolds with dipyridamole release for small diameter vascular grafts, Acta Biomater. 10 (2014) 4618–4628.
[18] I. Navarro-Baena, J.M. Kenny, L. Peponi, Crystallization and thermal characterization of biodegradable tri-block copolymers and poly(ester-urethane)s based on PCL and PLLA, Polym. Degrad. Stab. 108 (2014) 140–150.
[19] D. Cohn, A.F. Salomon, Designing biodegradable multiblock PCL/PLA thermoplastic elastomers, Biomaterials 26 (2005) 2297–2305.
[20] C. Xu, Y. Huang, J. Wu, L. Tang, Y. Hong, Triggerable degradation of polyurethanes for tissue engineering applications, ACS Appl. Mater. Interfaces 7 (2015) 20377–20388.
[21] J.J. Guan, M.S. Sacks, E.J. Beckman, W.R. Wagner, Synthesis, characterization, and cytocompatibility of efastomeric, biodegradable poly(ester-urethane)ureas based on poly(caprolactone) and putrescine, J. Biomed. Mater. Res. 61 (2002) 493–503.
[22] J.J. Guan, M.S. Sacks, E.J. Beckman, W.R. Wagner, Biodegradable poly(ether ester urethane)urea elastomers based on poly(ether ester) triblock copolymers and putrescine: synthesis, characterization and cytocompatibility, Biomaterials 25 (2004) 85–96.
[23] D. Cohn, T. Stern, M.F. Gonzalez, J. Epstein, Biodegradable poly(ethylene oxide)/poly(epsilon-caprolactone) multiblock copolymers, J. Biomed. Mater. Res. 59 (2002) 273–281.
[24] B. Guo, P.X. Ma, Synthetic biodegradable functional polymers for tissue engineering: a brief review, Sci. China Chem. 57 (2014) 490–500.
[25] B.D. Ulery, L.S. Nair, C.T. Laurencin, Biomedical applications of biodegradable polymers, J. Polym. Sci. Part B Polym. Phys. 49 (2011) 832–864.
[26] S. Baudis, S.C. Ligon, K. Seidler, G. Weigel, C. Grasl, H. Bergmeister, H. Schima, R. Liska, Hard-block degradable thermoplastic urethane-elastomers for electrospun vascular prostheses, J. Polym. Sci. Part A Polym. Chem. 50 (2012) 1272–1280.
[27] W. Lei, C. Fang, X. Zhou, J. Li, R. Yang, Z. Zhang, D. Liu, Thermal properties of polyurethane elastomer with different flexible molecular chain based on para-phenylene diisocyanate, J. Mater. Sci. Technol. 33 (2017) 1424–1432.
[28] F. Khan, S. Valere, S. Fuhrmann, V. Arrighi, M. Bradley, Synthesis and cellular compatibility of multi-block biodegradable poly(epsilon-caprolactone)-based polyurethanes, J. Mater. Chem. B 1 (2013) 2590–2600.
[29] C. Xu, Y. Huang, L. Tang, Y. Hong, Low-initial-modulus biodegradable polyurethane elastomers for soft tissue regeneration, ACS Appl. Mater. Interfaces 9 (2017) 2169–2180.
[30] M. Ding, Z. Qian, J. Wang, J. Li, H. Tan, Q. Gu, Q. Fu, Effect of PEG content on the properties of biodegradable amphiphilic multiblock poly(epsilon-caprolactone urethane)s, Polym. Chem. 2 (2011) 885–891.
[31] S. Li, C. Ye, G. Zhao, M. Zhang, Y. Zhao, Synthesis and properties of monocleavable amphiphilic comblike copolymers with alternating PEG and PCL grafts, J. Polym. Sci. Part A Polym. Chem. 50 (2012) 3135–3148.
[32] G. Zhao, X. Zhang, T.J. Lu, F. Xu, Recent advances in electrospun nanofibrous scaffolds for cardiac tissue engineering, Adv. Funct. Mater. 25 (2015) 5726–5738.
[33] T. Jiang, E.J. Carbone, K.W.H. Lo, C.T. Laurencin, Electrospinning of polymer nanofibers for tissue regeneration, Prog. Polym. Sci. 46 (2015) 1–24.
[34] X. Ren, Y. Feng, J. Guo, H. Wang, Q. Li, J. Yang, X. Hao, J. Lv, N. Ma, W. Li, Surface modification and endothelialization of biomaterials as potential scaffolds for vascular tissue engineering applications, Chem. Soc. Rev. 44 (2015) 5680–5742.
[35] Y. Naito, T. Shinoka, D. Duncan, N. Hibino, D. Solomon, M. Cleary, A. Rathore, C. Fein, S. Church, C. Breuer, Vascular tissue engineering: Towards the next generation vascular grafts, Adv. Drug Deliv. Rev. 63 (2011) 312–323.
[36] S.A. Sell, G.L. Bowlin, Creating small diameter bioresorbable vascular grafts through electrospinning, J. Mater. Chem. 18 (2008) 260–263.
[37] R.A. Hoshi, R. Van Lith, M.C. Jen, J.B. Allen, K.A. Lapidos, G. Ameer, The blood and vascular cell compatibility of heparin-modified ePTFE vascular grafts, Biomaterials 34 (2013) 30–41.
[38] D. Li, Y.N. Xia, Electrospinning of nanofibers: Reinventing the wheel? Adv. Mater. 16 (2004) 1151–1170.
[39] J.A. Matthews, G.E. Wnek, D.G. Simpson, G.L. Bowlin, Electrospinning of collagen nanofibers, Biomacromolecules 3 (2002) 232–238.
[40] Q.P. Pham, U. Sharma, A.G. Mikos, Electrospinning of polymeric nanofibers for tissue engineering applications: A review, Tissue Eng. 12 (2006) 1197–1211.

[41] D. Li, Y.L. Wang, Y.N. Xia, Electrospinning of polymeric and ceramic nanofibers as uniaxially aligned arrays, Nano Lett. 3 (2003) 1167–1171.
[42] T. Subbiah, G.S. Bhat, R.W. Tock, S. Pararneswaran, S.S. Ramkumar, Electrospinning of nanofibers, J. Appl. Polym. Sci. 96 (2005) 557–569.
[43] A. Haider, S. Haider, I.-K. Kang, A comprehensive review summarizing the effect of electrospinning parameters and potential applications of nanofibers in biomedical and biotechnology, Arab. J. Chem. 11 (2018) 1165–1188.
[44] X. Hu, S. Liu, G. Zhou, Y. Huang, Z. Xie, X. Jing, Electrospinning of polymeric nanofibers for drug delivery applications, J. Control. Release 185 (2014) 12–21.
[45] Y. Wang, S. Chen, Y. Pan, J. Gao, D. Tang, D. Kong, S. Wang, Rapid in situ endothelialization of a small diameter vascular graft with catalytic nitric oxide generation and promoted endothelial cell adhesion, J. Mater. Chem. B 3 (2015) 9212–9222.
[46] G.-H. Yang, F. Mun, G. Kim, Direct electrospinning writing for producing 3D hybrid constructs consisting of microfibers and macro-struts for tissue engineering, Chem. Eng. J. 288 (2016) 648–658.
[47] N. Isayama, G. Matsumura, H. Sato, S. Matsuda, K. Yamazaki, Histological maturation of vascular smooth muscle cells in in situ tissue-engineered vasculature, Biomaterials 35 (2014) 3589–3595.
[48] Y. Shirosaki, T. Okayama, K. Tsuru, S. Hayakawa, A. Osaka, Synthesis and cytocompatibility of porous chitosan-silicate hybrids for tissue engineering scaffold application, Chem. Eng. J. 137 (2008) 122–128.
[49] J. Horakova, P. Mikes, A. Saman, T. Svarcova, V. Jencova, T. Suchy, B. Heczkova, S. Jakubkova, J. Jirousova, R. Prochazkova, Comprehensive assessment of electrospun scaffolds hemocompatibility, Mater. Sci. Eng. C Mater. Biol. Appl. 82 (2018) 330–335.
[50] F. Xu, J.C. Nacker, W.C. Crone, K.S. Masters, The haemocompatibility of polyurethane-hyaluronic acid copolymers, Biomaterials 29 (2008) 150–160.
[51] T. Yokota, H. Ichikawa, G. Matsumiya, T. Kuratani, T. Sakaguchi, S. Iwai, Y. Shirakawa, K. Torikai, A. Saito, E. Uchimura, N. Kawaguchi, N. Matsuura, Y. Sawa, In situ tissue regeneration using a novel tissue-engineered, small-caliber vascular graft without cell seeding, J. Thorac. Cardiovasc. Surg. 136 (2008) 900–907.
[52] J. Li, M. Ding, Q. Fu, H. Tan, X. Xie, Y. Zhong, A novel strategy to graft RGD peptide on biomaterials surfaces for endothelization of small-diamater vascular grafts and tissue engineering blood vessel, J. Mater. Sci. Mater. Med. 19 (2008) 2595–2603.
[53] T. Zhu, H. Gu, H. Zhang, H. Wang, H. Xia, X. Mo, J. Wu, Covalent grafting of PEG and heparin improves biological performance of electrospun vascular grafts for carotid artery replacement, Acta Biomater. 119 (2021) 211–224.